

## Article

# Risk Assessment of Freezing–Thawing Hazards in the Daxing’anling Forest Region

Kezheng Chen <sup>1,\*</sup>  and Shuai Huang <sup>2</sup><sup>1</sup> College of Mechanical and Electrical Engineering, Northeast Forestry University, Harbin 150040, China<sup>2</sup> College of Forestry, Northeast Forestry University, Harbin 150040, China; s\_hwang@nefu.edu.cn

\* Correspondence: chenkezheng@nefu.edu.cn

**Abstract:** The Daxing’anling forest region represents a crucial forestry hub in China and confronts some of the nation’s most severe freezing–thawing hazards. This study delved into the temporal trends and spatial distributions of various parameters related to freezing and thawing, including air temperature, ground surface temperature, freezing index, thawing index, and freezing–thawing frequency. Furthermore, this study assessed and delineated freezing–thawing hazards within the research area. The findings revealed a rapid increase in air temperature and ground surface temperature within the Daxing’anling forest region yet a lower rate of increase in ground surface temperature compared to Northeast China. Latitude had the strongest influence on mean annual air temperature, mean annual ground surface temperature, air freezing index, air thawing index, ground surface freezing index, ground surface thawing index, air freezing–thawing frequency, and ground surface freezing–thawing frequency, followed by longitude and elevation. Overall, freezing index, and air freezing–thawing frequency increased from south to north, whereas mean annual air temperature, mean annual ground surface temperature, air thawing index, ground surface thawing index, and ground surface freezing–thawing frequency decreased from south to north. The assessment outcomes underscore the importance of closely monitoring freezing–thawing hazards in regions north of the 50th parallel.

**Keywords:** Daxing’anling forest region; air temperature; ground surface temperature; freezing–thawing index; freezing–thawing frequency; entropy weight–TOPSIS model



**Citation:** Chen, K.; Huang, S. Risk Assessment of Freezing–Thawing Hazards in the Daxing’anling Forest Region. *Atmosphere* **2023**, *14*, 1721. <https://doi.org/10.3390/atmos14121721>

Academic Editors: Tin Lukić and Alexey V. Eliseev

Received: 5 October 2023

Revised: 5 November 2023

Accepted: 20 November 2023

Published: 23 November 2023



**Copyright:** © 2023 by the authors. Licensee MDPI, Basel, Switzerland. This article is an open access article distributed under the terms and conditions of the Creative Commons Attribution (CC BY) license (<https://creativecommons.org/licenses/by/4.0/>).

## 1. Introduction

The Daxing’anling forest region is a critical element of the Xing’anling and serves as China’s northernmost ecological security barrier [1]. In recent years, substantial construction initiatives have unfolded in the Daxing’anling forest region, including the China–Russia crude oil pipeline (CRCOP), along with associated highways, airports, railways, and forestry roads [2–4]. In the context of the Belt and Road Initiative and the revitalization of Northeast China, the pace of construction in the Daxing’anling forest region is poised to accelerate [5,6]. This region encompasses the Xing’an–Baikal permafrost, which is rapidly deteriorating due to the combined impacts of climate change and human activities [7–11]. Permafrost degradation can lead to ground settlement and uneven subsidence in the foundations of engineering projects [4,12]. Moreover, this area experiences one of the highest frequencies of freezing–thawing cycles, capable of causing damage to existing and forthcoming construction endeavors [13–16]. To forecast permafrost degradation and mitigate freezing–thawing damage, a comprehensive examination of air temperature, ground surface temperature, freezing–thawing indices, and freezing–thawing frequencies in the Daxing’anling forest region is imperative. These investigations underpin the theoretical basis for engineering construction and maintenance in this locality.

To assess various proposals, techniques such as the analytic hierarchy process (AHP), fuzzy comprehensive evaluation, and Technique for Order of Preference by Similarity to

Ideal Solution (TOPSIS) are conventionally employed [17–20]. AHP is straightforward but may involve qualitative aspects that prove challenging to discern quantitatively. Fuzzy comprehensive evaluation enables the quantitative evaluation of fuzzy data with concealed information but entails computational complexity and is susceptible to subjectivity. In contrast, TOPSIS objectively gauges proposal superiority using Euclidean distance, featuring a simpler computational process and greater versatility in evaluating proposal excellence. To allocate weights to proposal factors, objective weighting methods, such as the coefficient of variation, entropy weight, and CRITIC method, are frequently employed [21–23]. Among these, the entropy weight method eliminates the need for deliberate indicator selection and provides a straightforward way to standardize various factors. Consequently, this study employed the entropy weight–TOPSIS model to assess and categorize freezing–thawing hazards in the Daxing’anling forest region [24,25].

To this end, we selected air temperature and ground surface temperature data from 38 meteorological stations in and around the Daxing’anling forest region in the period of 2005–2020. Employing these data, freezing indices, thawing indices, and freezing–thawing frequencies were computed. Subsequently, temporal trends and spatial distribution patterns were analyzed. Ultimately, freezing–thawing hazards in the Daxing’anling forest region were assessed and categorized with the entropy weight–TOPSIS model, and priority regions for freezing–thawing hazard prevention and management within the study area were delineated.

## 2. Materials and Methods

### 2.1. Study Area

The Daxing’anling forest region is located primarily in the Daxing’anling area of Heilongjiang Province and Hulunbuir in Inner Mongolia. Its geographical coordinates span from approximately 50°05' N to 53°34' N in latitude and from 121°41' E to 127°10' E in longitude (Figure 1). Encompassing an area of roughly  $8.4 \times 10^4$  km<sup>2</sup>, it is one of China’s significant forestry hubs and is the sole natural coniferous forest region in China [26]. The study area falls within the geomorphological classification of low hills and ridges of glacial origin. The geological formations primarily comprise Jurassic and Cretaceous volcanic rocks, featuring materials such as basalt, sandy shale, and granite [26]. Mount Xing’an Motian is the highest point in the research area, at an elevation of 1712 m, while the lowest elevation is found in Yanjiang Village, Sanka Township, Hu’ma County, at 180 m above sea level (Figure 1b). The predominant soil type in the study area is brown coniferous forest soil [27]. The study area experiences a subarctic continental monsoon climate, characterized by an annual average temperature below 0 °C [27–29]. Influenced by both continental and oceanic monsoons, the climate exhibits a wide range of variation, with significant local disparities. Winters in the region are prolonged, arid, and exceedingly cold, with temperatures plummeting to below –50 °C. In contrast, summers are marked by high humidity and concentrated and ample rainfall, with an annual average precipitation of approximately 450 mm. The research area boasts an extensive river network, serving as the headwaters of the Heilongjiang and Songhua Rivers. There are permafrost layers and high groundwater levels within the region [30,31].

### 2.2. Data Sources

The ground surface temperature, air temperature, and precipitation data utilized in this study were acquired from the China Meteorological Data Service Centre “<http://data.cma.cn/> (accessed on 25 April 2023)”. In this context, air temperature refers to the air temperature inside a louvered box located 1.5 m above the ground, while ground temperature refers to the temperature at a depth of 0 cm. Digital elevation data are sourced from the Geospatial Data Cloud “<https://www.gscloud.cn/> (accessed on 26 April 2023)” and used to derive slope data. Mean annual snow cover duration was obtained from the National Tibetan Plateau Data Center “<https://data.tpdc.ac.cn/> (accessed on 25 October 2023)”. Normalized difference vegetation index (NDVI) data originated from the Resource and Environmental



$$TI = \sum_{i=1}^{N_f} |T_i|, T_i > 0 \tag{3}$$

where *FI* refers to the annual freezing index (°C×d), which comprises the air freezing index (AFI) and ground surface freezing index (GFI). *TI* denotes the annual thawing index (°C×d), which includes the air thawing index (ATI) and ground surface thawing index (GTI). *T<sub>i</sub>* represents the daily average air temperature or ground surface temperature, *N<sub>f</sub>* represents the number of continuous days with temperatures below 0 °C, and *N<sub>t</sub>* represents the number of continuous days with temperatures above 0 °C.

### 2.3.3. Freezing–Thawing Frequency

One freezing–thawing cycle is defined as a day when the maximum ground surface temperature (air temperature) rises above 0 °C, while the minimum ground surface temperature (air temperature) drops below 0 °C. The annual tally of such freezing–thawing cycles is regarded as the freezing–thawing frequency for that year [35]. The freezing–thawing frequency was ascertained through the analysis of daily observations of maximum ground surface temperature (air temperature) and minimum ground surface temperature (air temperature).

### 2.3.4. Entropy Weight–TOPSIS Model

TOPSIS is a computationally efficient and scientifically rigorous decision-making method. It is commonly employed for multi-objective decision analysis in scenarios with multiple available options and has been extensively applied in assessment and decision-making processes across various domains [17,36,37]. Utilizing the entropy weight method to assign values to each factor, the entropy weight–TOPSIS model has been established based on TOPSIS theory [21,38–41]. We employed this model to assess and rank the freezing–thawing hazards experienced by meteorological stations within the study area and to subsequently evaluate the spatial distribution of freezing–thawing events in the Daxing’anling forest region. The steps involved in constructing the entropy weight–TOPSIS model were as follows:

#### 1. Building the index system

Several relevant parameters were chosen as evaluation indices for the model based on the assessment objective to establish the assessment index system.

#### 2. Building an initial matrix

For assessing *m* objects using *n* evaluation indicators, an initial matrix *A* was formed.

$$A = (a_{ij})_{n \times m}, (i = 1, 2, \dots, n; j = 1, 2, \dots, m).$$

#### 3. Building a standardized decision matrix

To mitigate the influence of evaluation results caused by scale differences, the indicators underwent dimensionless processing. The standardized matrix *B* was derived by either normalizing or inverting the initial matrix *A*. *B* = (*b<sub>ij</sub>*)<sub>*n* × *m*</sub>, (*i* = 1, 2, . . . , *n*; *j* = 1, 2, . . . , *m*).

The dimensionless treatment was as follows [25]:

Positive normalization was applied to metrics with higher attribute values:

$$b_{ij} = \frac{a_{ij} - \min a_j}{\max a_j - \min a_j} \tag{4}$$

Negative normalization was applied to metrics with lower attribute values:

$$b_{ij} = \frac{\max a_j - a_{ij}}{\max a_j - \min a_j} \tag{5}$$

- Determination of the weights of the indices using the entropy weighting method [21].

Entropy value of each index:

$$H_{ij} = -\frac{1}{\ln m} \sum_{i=1}^m f_{ij} \ln f_{ij} \tag{6}$$

where  $f_{ij} = \frac{b_{ij}}{\sum_{i=1}^m b_{ij}}$ , when  $f_{ij} = 0, f_{ij} \ln f_{ij} = 0$ .

Entropy weights for each index:

$$w_j = \frac{1 - H_j}{n - \sum_{j=1}^n H_j}, 0 \leq w_j \leq 1, \sum_{j=1}^n w_j = 1 \tag{7}$$

- Establishment of a weighted standardization matrix [25]

The weighted normalization matrix **C** was obtained by multiplying the normalization matrix **B** and the weights  $w_j$ .  $C = (c_{ij})_{n \times m}$ .

$$c_{ij} = b_{ij} \times w_j \tag{8}$$

- Determining the ideal solution [25]

Positive ideal solution:

$$D^+ = \left( \max_{1 \leq i \leq m} y_{ij} \mid j \in j^+, \min_{1 \leq i \leq m} y_{ij} \mid j \in j^- \right) = (d_1^+, d_2^+, \dots, d_n^+) \tag{9}$$

Negative ideal solution:

$$D^- = \left( \min_{1 \leq i \leq m} y_{ij} \mid j \in j^+, \max_{1 \leq i \leq m} y_{ij} \mid j \in j^- \right) = (d_1^-, d_2^-, \dots, d_n^-) \tag{10}$$

- Determining the Euclidean distance [25]

Euclidean distance to the positive ideal solution for each evaluated object:

$$E_i^+ = \sqrt{\sum_{j=1}^n (y_{ij} - d_j^+)^2} \quad (i = 1, 2, \dots, m) \tag{11}$$

Euclidean distance to the negative ideal solution for each evaluated object:

$$E_i^- = \sqrt{\sum_{j=1}^n (y_{ij} - d_j^-)^2} \quad (i = 1, 2, \dots, m) \tag{12}$$

- Program score [25]

$$F_i = \frac{E_i^-}{E_i^+ + E_i^-} \quad (i = 1, 2, \dots, m) \tag{13}$$

Finally, the intensity of the freezing–thawing hazard was evaluated for each subject based on the score it received.

### 2.3.5. Pearson’s Correlation Coefficient

Pearson’s correlation coefficient was used to assess the linear relationships between each index. Equation (14) presents the method of calculating Pearson’s correlation coefficient [42].

$$r_{jk} = \frac{\sum_{i=1}^m (b_{ij} - \bar{b}_j)(b_{ik} - \bar{b}_k)}{\sqrt{\sum_{i=1}^m (b_{ij} - \bar{b}_j)^2} \sqrt{\sum_{i=1}^m (b_{ik} - \bar{b}_k)^2}}, i = 1, 2, \dots, m; j = 1, 2, \dots, n; k = 1, 2, \dots, n \quad (14)$$

where  $j$  represents the mean value of the  $j$ th index in the standardized matrix and  $b_k$  represents the mean value of the  $k$ th index in the standardized matrix.

## 3. Results

### 3.1. Changes in Air Temperature and Ground Surface Temperature

For the 2005–2020 period, multi-year annual average temperature calculations were performed for 38 meteorological stations within and around the Daxing’anling forest region. This yielded the temporal evolution pattern of the mean annual air temperature (MAAT), as depicted in Figure 2. The MAAT in the study area showed an increasing trend with a growth rate of 0.047 °C/a. During the 2005–2020 period, the lowest recorded temperature occurred in 2012 (−0.23 °C), while the highest was observed in 2007 (2.10 °C). The average value for the 2005–2020 years was 0.94 °C.

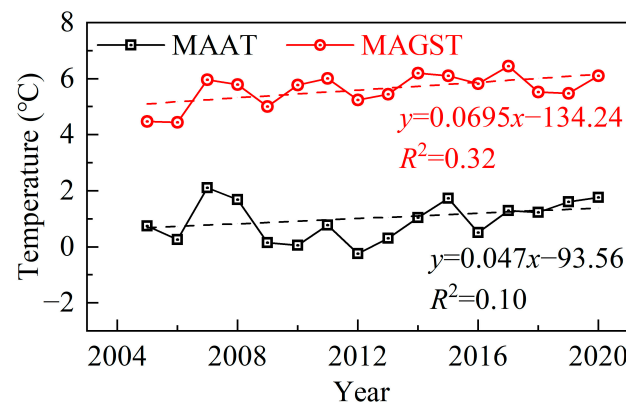


Figure 2. Changes in the MAAT and MAGST in the Daxing’anling forest region.

The temporal trend of the mean annual ground surface temperature (MAGST) in the study area (Figure 2) closely mirrored the temperature trend. It exhibited an ascending pattern with a growth rate of 0.0695 °C/a. The highest recorded temperature occurred in 2017 (6.45 °C), while the lowest was observed in 2006 (4.44 °C). The average value for the 2005–2020 years was 5.62 °C.

The spatial distributions of MAAT and the air temperature change rate (ATCR) in the study area are illustrated in Figure 3. The northern and central mountainous areas displayed the lowest temperatures, whereas the southern region (near the Songnen Plain) recorded the highest temperatures. Furthermore, an analysis of the relationship between MAAT and longitude, latitude, and altitude (Equation (15)) revealed that MAAT had a strong correlation with latitude, a moderate correlation with longitude, and a weak correlation with altitude. The ATCR exhibited the opposite pattern: the farther north, the more intense the warming, with the western grassland areas experiencing relatively stable temperatures. However, in the northeastern corner of the study area (Hu’ma), a cooling trend was observed.

$$MAAT = -0.2153Long - 1.0265Lat - 0.0085Alt + 81.4101(R^2 = 0.96, p < 0.05) \quad (15)$$

where *Long* is the longitude (°), *Lat* is the latitude (°), and *Alt* is the altitude (m).

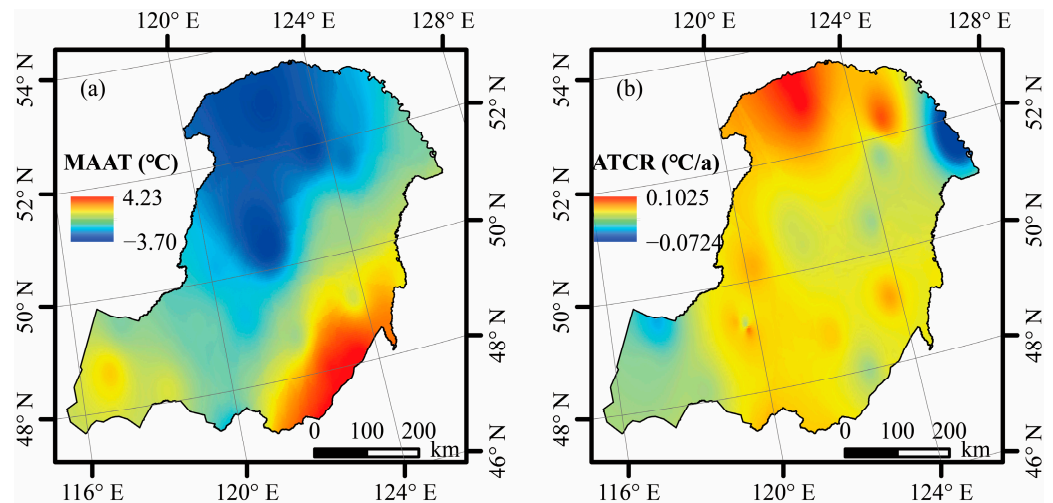


**Figure 3.** Spatial distributions of the MAAT (a) and ATCR (b) in the Daxing'anling forest region.

The spatial distributions of MAGST and the ground surface temperature change rate (GSTCR) in the study area are depicted in Figure 4. The northern and central mountainous areas displayed the lowest ground surface temperatures, whereas the southern region (near the Songnen Plain) recorded the highest ground surface temperatures. The evaluation of the influence of longitude, latitude, and altitude on MAGST (Equation (16)) revealed that latitude was the primary influencing factor, followed by longitude, while altitude exerted the lowest effect on MAGST. Close to Beijicun, the ground surface temperature rose the most rapidly, whereas in the western grassland areas and the northeastern region near the Heilongjiang River, a cooling trend in ground surface temperature was observed.

$$MAGST = -0.0344Long - 0.7058Lat - 0.0043Alt + 46.3599 (R^2 = 0.91, p < 0.05) \quad (16)$$

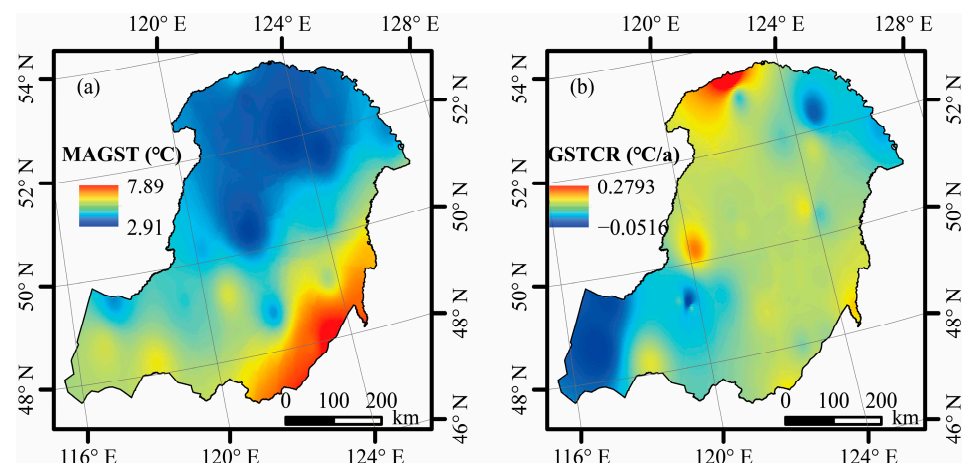


**Figure 4.** Spatial distributions of the MAGST (a) and GSTCR (b) in the Daxing'anling forest region.

### 3.2. Changes in Freezing Index and Thawing Index

The calculations for the 38 meteorological stations in the study area, including the AFI, air freezing index change rate (AFICR), ATI, air thawing index change rate (ATICR), GFI, ground freezing index change rate (GFICR), GTI, and ground thawing index change rate (GTICR) in 2005–2020, were performed to evaluate their temporal and spatial variations.

Across the entire Daxing'anling forest region, the AFI (Figure 5) exhibited a fluctuating downward trend, with the lowest value in 2018 (2031.82 °C×d) and the highest in 2012

(2986.77 °C×d). The average was 2490.41 °C×d, with a change rate of −12.79 °C×d/a. In contrast, the ATI (Figure 5) showed a fluctuating upward trend, with the lowest value in 2006 (2722.02 °C×d) and the highest in 2018 (2969.91 °C×d). The average was 2825.89 °C×d, with a change rate of 3.06 °C×d/a.

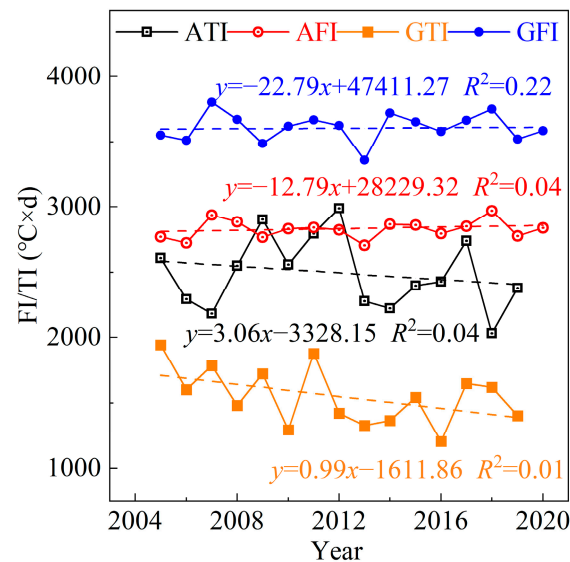


Figure 5. Changes in the AFI, ATI, GFI, and GTI in the Daxing’anling forest region.

The entire Daxing’anling forest region displayed a fluctuating decreasing trend in the GFI (Figure 5). The lowest value occurred in 2016 (1207.10 °C×d), while the highest value was observed in 2005 (1943.28 °C×d). The average GFI was 1549.47 °C×d, with a change rate of −22.79 °C×d/a. The GTI (Figure 5) exhibited a fluctuating increasing trend. The lowest value was recorded in 2013 (3357.79 °C×d), while the highest value was observed in 2007 (3802.60 °C×d). The average GTI was 3609.91 °C×d, with a change rate of 0.99 °C×d/a.

The spatial distributions of the AFI, AFICR, ATI, and ATICR in the Daxing’anling forest region are depicted in Figure 6. As shown in Figure 6a, the AFI was higher in the northern and central parts of the Daxing’anling forest region than in the southern parts. In the southern region, closer to the Songnen Plain, the AFI was the lowest, followed by the southwestern Hulunbuir Plateau. When analyzing the influence of latitude, longitude, and elevation on AFI (Equation (17)), latitude had the greatest effect, followed by longitude, while elevation had the weakest effect. When examining AFICR, the most significant AFI reduction was observed in the northern part of the study area, specifically in Beijicun, Mo’he, and Ta’he. In contrast, variation in the AFI in Hu’ma, the southern area near the Songnen Plain, and the Hulunbuir Plateau was relatively small.

$$AFI = 18.99Long - 237.82Lat - 1.38Alt + 12124.81 (R^2 = 0.89, p < 0.05) \quad (17)$$

The distribution patterns of the ATI exhibited an opposite trend to those of the AFI. The ATI was lower in the northern and central mountainous areas, while in the southern parts of the study area, closer to the Songnen Plain, it reached its highest values. In the southwestern Hulunbuir Plateau, the ATI was lower than in the southern areas of the Daxing’anling forest region near the Songnen Plain but higher than in the northern and central mountainous areas. As shown in Equation (18), latitude had the greatest influence on the ATI, followed by longitude, while elevation had the weakest effect. The distribution pattern of the ATICR was opposite to that of the AFICR. Spatially, the ATICR indicated

a decrease in the ATI in Hu'ma and parts of the Hulunbuir Plateau, while in most other regions, the ATI showed an increasing trend.

$$ATI = -59.55Long - 139.14Lat - 1.68Alt + 17682.57(R^2 = 0.97, p < 0.05) \quad (18)$$

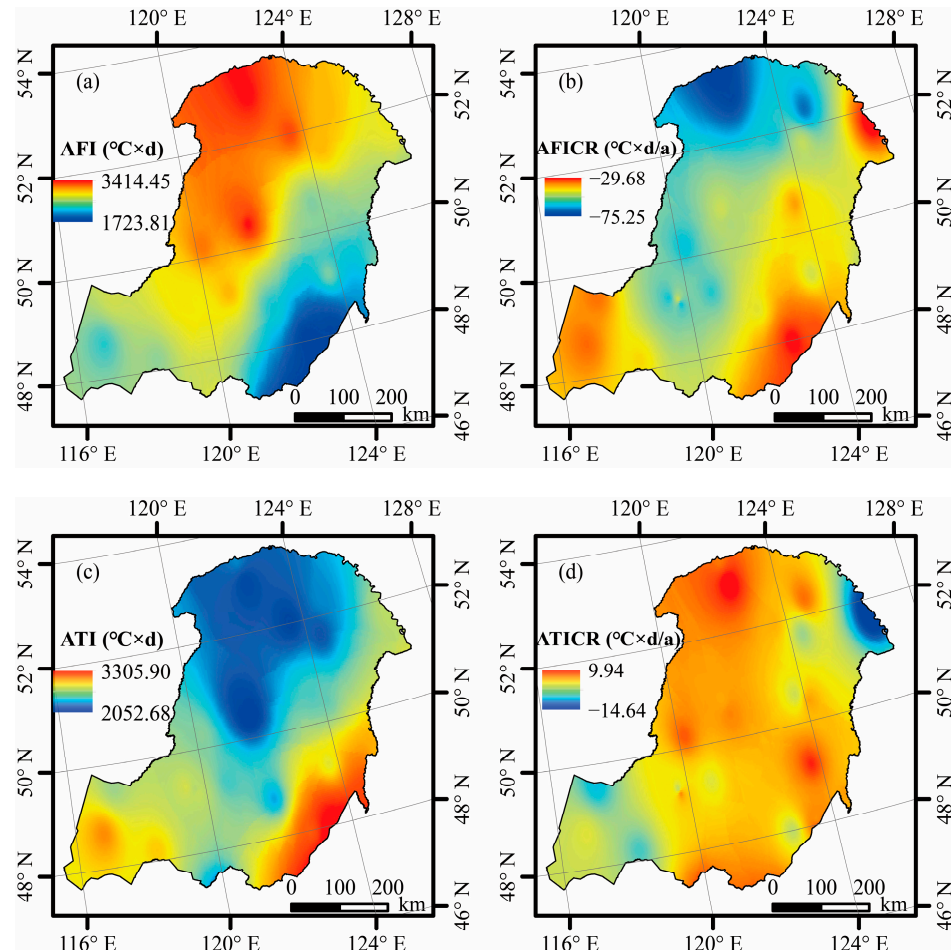


**Figure 6.** Spatial distributions of the AFI (a), AFICR (b), ATI (c), and ATICR (d) in the Daxing'anling forest region.

The spatial distributions of the GFI, GFICR, GTI, and GTICR in the Daxing'anling forest region are depicted in Figure 7. The GFI was influenced by snow cover, leading to significant differences in its spatial distribution compared to the AFI. In northeastern Hu'ma and western areas like Manzhouli and Ergunna, the AFI was relatively high, while in regions near the Songnen Plain, the AFI was lower. In the northern part of the study area, near Mo'he and Beijicun, the AFI was also lower due to the influence of snow cover. Based on the analysis (Equation (19)), latitude was an important factor affecting the GFI, followed by longitude, while elevation had the lowest effect. Figure 7b reveals that the spatial distribution pattern of the GFICR was less regular. The GFICR was relatively low in the vicinity of the Heilongjiang and Songhua Rivers, indicating that rivers had a significant effect on variation in the GFI.

$$GFI = -60.31Long + 96.34Lat - 0.19Alt + 4289.91(R^2 = 0.46, p < 0.05) \quad (19)$$

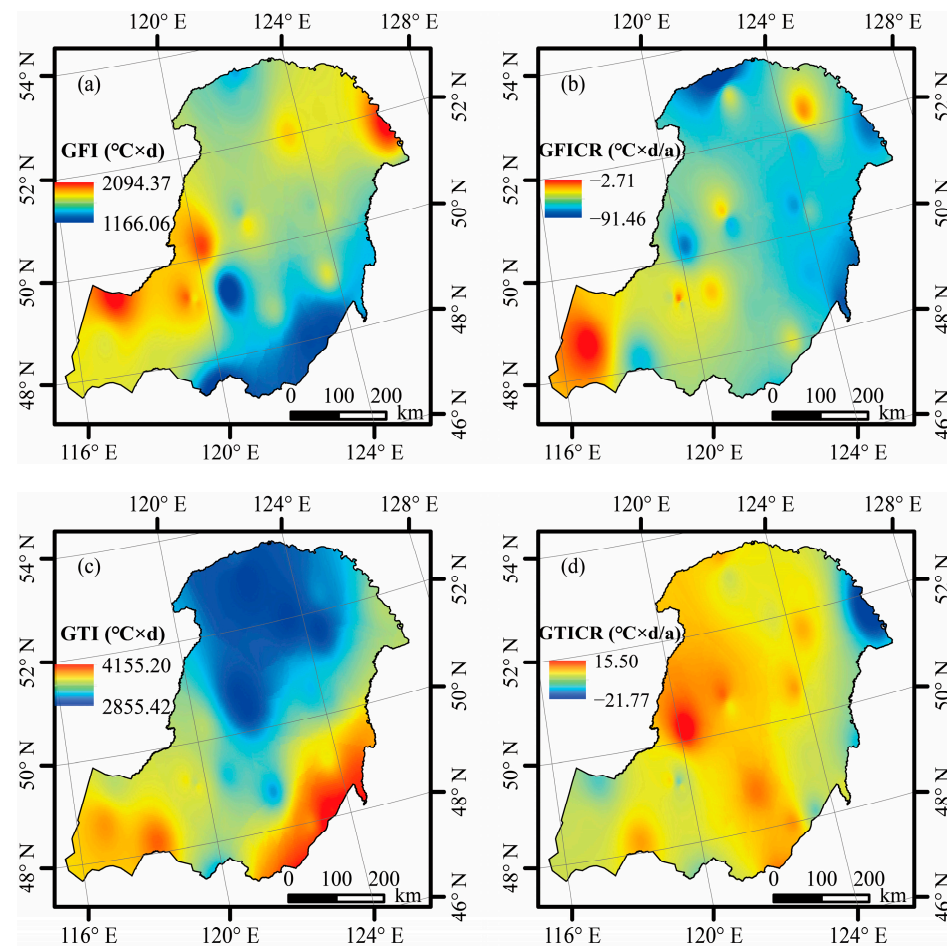


**Figure 7.** Spatial distributions of the GFI (a), GFICR (b), GTI (c), and GTICR (d) in the Daxing'anling forest region.

The distribution pattern of the GTI closely mirrored that of the ATI, with lower values in the northern and central mountainous areas, higher values in the southern part of the study area, and lower values in the Hulunbuir Plateau compared to the southern part of the study area but higher than in the northern and central mountainous areas. As per Equation (20), it is evident that latitude had the most significant influence on the GTI, while elevation had the lowest effect, and the effect of longitude on the GTI fell between those of latitude and elevation. The distribution pattern of the GTICR within the study area remained consistent with that of the ATICR but exhibited greater variation.

$$GTI = -74.46Long - 162.91Lat - 1.77Alt + 21507.14(R^2 = 0.95, p < 0.05) \quad (20)$$

### 3.3. Changes in Freezing–Thawing Frequency

The air freezing–thawing frequency (AFTF) in the Daxing'anling forest region, as depicted in Figure 8, showed an oscillating upward trend, with the lowest value recorded in 2012 (59) and the highest in 2019 (93). The average AFTF was 73 th/a, with a rate of change of 0.48 th/a.

In contrast, the ground freezing–thawing frequency (GFTF) in the Daxing'anling forest region, as illustrated in Figure 8, exhibited a fluctuating declining trend. The lowest value was observed in 2013 (78), while the highest value was recorded in 2019 (116). The annual average was 97 th/a, with a change rate of  $-0.75$  th/a.

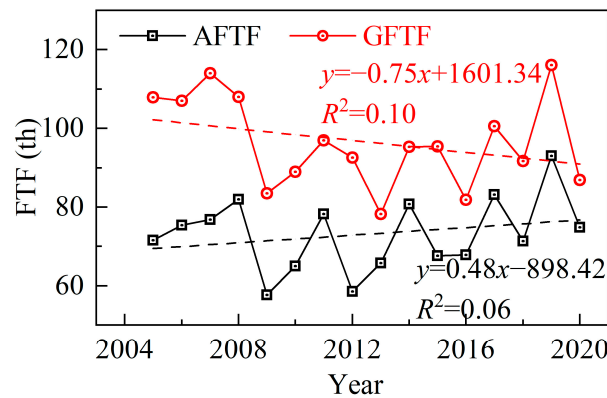


Figure 8. Changes in the AFTF and GFTF in the Daxing’anling forest region.

The spatial distributions of the AFTF and its rate of change (AFTFCR) in the Daxing’anling forest region are depicted in Figure 9. In the northern and central mountainous regions of the study area, the AFTF was higher than in the southern region, with the lowest values observed in the southeastern region near the Songnen Plain and the southwestern area near the Hulunbuir Plateau. Multiple linear regression analysis (Equation (21)) revealed that latitude was the primary factor influencing the AFTF, followed by longitude, with altitude having the weakest effect. When examining the distribution of the AFTFCR, most regions exhibited an increasing trend in the AFTF, which was particularly noticeable around Hu’ma, Manzhouli, Arun Banner, and Jagdaqi. In contrast, in some parts of the northern and central areas of the study area, the AFTFCR was less than 0, indicating a decrease in the AFTF in those regions.

$$AFTF = 1.3855Long + 3.2533Lat + 0.0393Alt - 273.4415 (R^2 = 0.54, p < 0.05) \quad (21)$$

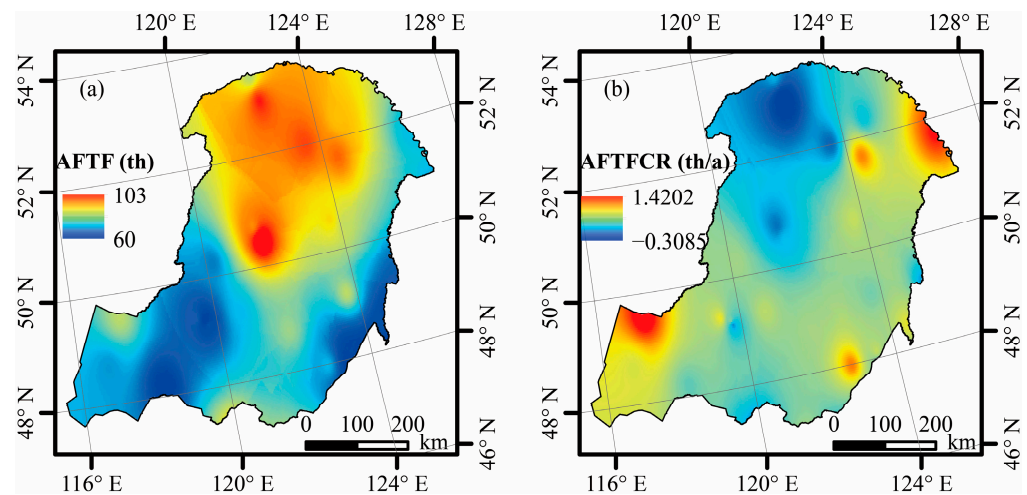


Figure 9. Spatial distributions of the AFTF (a) and AFTFCR (b) in the Daxing’anling forest region.

The spatial distributions of the GFTF and its change rate (GFTFCR) in the Daxing’anling forest region are illustrated in Figure 10. Due to the influence of snow cover, the distribution pattern of the GFTF did not resemble that of the AFTF. The GFTF showed a decreasing trend from south to north, with the highest values occurring south of Arun Banner. In certain areas, such as Mo’he and Hu’ma, the GFTF values were lower than in other areas. The GFTF values near Hulun Lake were relatively high but lower than those south of Boketu. Multiple linear regression analysis (Equation (22)) revealed that latitude was the primary factor influencing the GFTF, followed by longitude, with altitude having the weakest effect. When examining the spatial distribution of the GFTFCR, the GFTF rapidly decreased in the central part of the study area and in Hu’ma. In contrast, the GFTF

increased at a faster rate in places like Manzhouli, while the change in the GFTF in other areas was relatively gradual.

$$GFTF = -1.8747Long - 4.6141Lat - 0.0127Alt + 559.3272 (R^2 = 0.44, p < 0.05) \quad (22)$$

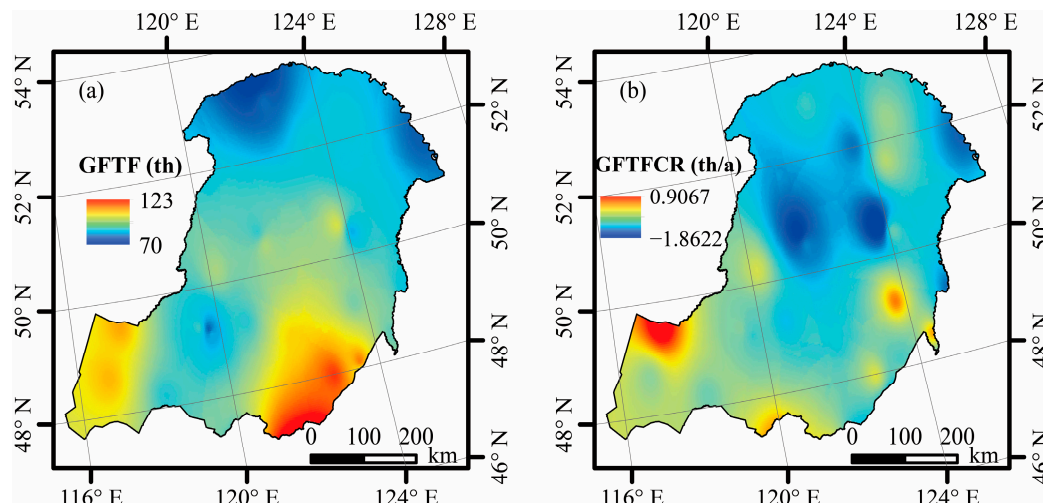


Figure 10. Spatial distributions of the GFTF (a) and GFTFCR (b) in the Daxing'anling forest region.

### 3.4. Freezing–Thawing Hazard Assessment in the Daxing'anling Forest Region

Based on the assessment objectives, we selected the following indices to evaluate freezing–thawing hazards in the study area: MAAT, MAGST, AFI, ATI, GFI, GTI, AFTF, GFTF, volume ice content of permafrost (VIC), slope (Slope), NDVI, mean annual precipitation (MAP), and mean annual snow cover duration (MASCD). Table 1 presents the values initially selected as evaluation indices.

Table 1. The values initially selected as evaluation indices for freezing–thawing hazard assessment in the Daxing'anling forest region.

Meteorological Station	MAAT	MAGST	AFI	ATI	GFI	GTI	AFTF	GFTF	VIC	Slope	NDVI	MAP	MASCD
50,136	−3.32	3.43	3414.51	2189.46	1605.26	2855.31	96.25	82.88	25	1.61	0.74	375.61	147.85
50,137	−2.81	4.20	3408.99	2364.00	1458.72	3052.93	80.50	69.44	33	0.25	0.63	375.94	168.95
50,246	−1.74	3.72	3016.88	2365.13	1773.41	3117.74	87.81	89.94	28	2.88	0.60	403.08	140.50
50,247	−3.05	2.91	3295.12	2174.28	1847.53	2884.56	94.50	90.31	39	6.22	0.76	402.71	158.45
50,349	−2.06	3.09	3017.50	2253.14	1770.88	2903.28	92.75	88.88	36	2.11	0.59	423.25	148.90
50,353	−0.17	3.89	2838.67	2752.66	2091.93	3499.50	71.63	81.63	18	0.28	0.65	392.64	140.00
50,425	−1.48	4.08	3184.90	2642.54	2018.53	3513.66	68.19	97.56	22	0.00	0.53	312.52	130.10
50,431	−2.92	3.49	3260.39	2201.34	1590.23	2895.78	90.75	91.38	35	1.02	0.48	387.39	141.05
50,434	−3.70	2.94	3401.33	2052.39	1810.50	2875.39	103.06	97.88	48	0.32	0.59	378.21	145.20
50,442	0.26	4.34	2508.31	2591.61	1724.55	3291.24	81.38	86.69	18	0.11	0.56	399.78	131.20
50,445	0.26	4.29	2479.19	2565.87	1624.36	3181.70	86.44	101.69	22	0.28	0.69	400.39	118.15
50,468	1.51	6.22	2392.05	2927.66	1280.75	3566.57	64.94	81.81	5	1.24	0.77	460.00	130.70
50,514	−0.12	3.92	2732.74	2679.91	2094.52	3513.50	80.88	109.69	8	0.55	0.56	219.06	112.50
50,524	−0.24	4.54	2896.56	2800.19	1977.97	3660.88	66.06	91.81	5	0.05	0.46	255.71	126.40
50,525	−0.27	4.81	2871.27	2767.51	1872.49	3650.46	65.13	86.63	5	0.12	0.46	277.06	131.85
50,526	−1.27	5.70	3015.79	2550.33	1174.96	3256.94	70.94	90.94	14	0.27	0.50	336.95	134.90
50,527	−0.33	4.71	2864.41	2734.33	1797.97	3520.50	60.88	82.13	2	4.10	0.67	261.04	133.00
50,548	1.04	5.19	2467.03	2841.26	1762.21	3650.66	80.94	94.31	10	0.09	0.65	395.34	111.30
50,557	1.43	6.32	2474.31	2982.02	1493.43	3800.08	66.19	88.38	6	0.25	0.48	405.38	109.15
50,564	1.31	6.86	2416.81	2883.55	1102.49	3614.98	69.31	85.19	15	0.00	0.71	448.46	128.45
50,603	1.95	5.60	2343.68	3048.65	1762.07	3824.59	69.31	108.44	0	0.70	0.34	172.40	100.15
50,618	1.17	5.90	2519.98	2946.81	1750.66	3927.04	61.31	90.69	6	0.43	0.40	209.98	117.25
50,632	0.26	3.96	2314.71	2406.83	1660.22	3132.87	78.69	106.75	17	5.91	0.77	377.20	124.85

Table 1. Cont.

Meteorological Station	MAAT	MAGST	AFI	ATI	GFI	GTI	AFTF	GFTF	VIC	Slope	NDVI	MAP	MASCD
50,639	3.89	6.89	1723.63	3136.83	1316.97	3849.68	70.88	116.94	0	0.21	0.38	364.02	57.25
50,645	2.95	6.88	2099.31	3164.91	1484.71	4011.84	65.13	93.00	0	0.78	0.78	389.71	102.55
50,646	2.80	6.86	2191.13	3203.26	1526.48	4064.40	58.13	95.38	0	0.19	0.54	394.94	106.95
50,647	3.90	7.30	1815.47	3227.45	1341.97	4024.26	63.38	112.56	0	0.71	0.81	359.86	86.05
50,655	1.10	6.27	2565.59	2944.39	1438.43	3767.26	68.31	82.63	8	0.36	0.71	422.38	125.20
50,658	2.65	6.91	2187.47	3146.58	1392.72	3929.49	55.56	96.88	0	1.25	0.80	413.27	113.85
50,727	-1.64	5.51	2835.91	2247.83	1026.23	3042.13	87.69	90.56	41	3.57	0.65	347.42	149.30
50,739	4.83	7.26	1652.61	3410.88	1398.04	4067.98	62.56	117.94	0	0.48	0.83	337.83	81.15
50,741	4.51	8.38	1725.24	3363.24	1184.59	4258.49	56.94	100.94	0	0.21	0.54	354.86	94.80
50,742	3.77	8.22	1941.35	3306.66	1249.91	4269.18	57.75	95.13	0	0.18	0.67	373.54	93.45
50,745	4.68	8.17	1784.03	3488.29	1261.14	4264.60	58.50	97.69	0	0.22	0.46	342.45	87.30
50,750	3.08	7.69	2090.99	3208.30	1132.92	3962.13	55.69	87.44	0	1.03	0.61	393.42	101.00
50,832	4.55	7.55	1630.53	3286.66	1385.62	4157.21	81.06	138.56	0	0.62	0.73	336.63	66.30
50,833	5.53	8.32	1514.20	3532.20	1315.75	4358.38	63.88	112.38	0	2.08	0.47	334.62	46.60
50,834	3.43	7.07	1742.93	2994.99	1378.67	3959.48	84.38	136.31	0	0.34	0.72	327.33	63.70

A scientific, rational, and accurate evaluation of the 13 selected indices was conducted using Pearson’s correlation coefficient. Figure 11 displays Pearson’s correlation coefficients among these 13 indices. Studies commonly acknowledge that when Pearson’s correlation coefficient exceeds 0.80, there is a strong correlation between two indices, making them unsuitable for simultaneous inclusion in the evaluation system. Based on Pearson’s correlation coefficients among the indices, eight indices were selected as the assessment criteria for freezing–thawing hazards within the study area. These selected indices were MAGST, GFI, GFTF, VIC, Slope, NDVI, MAP, and MASCD.

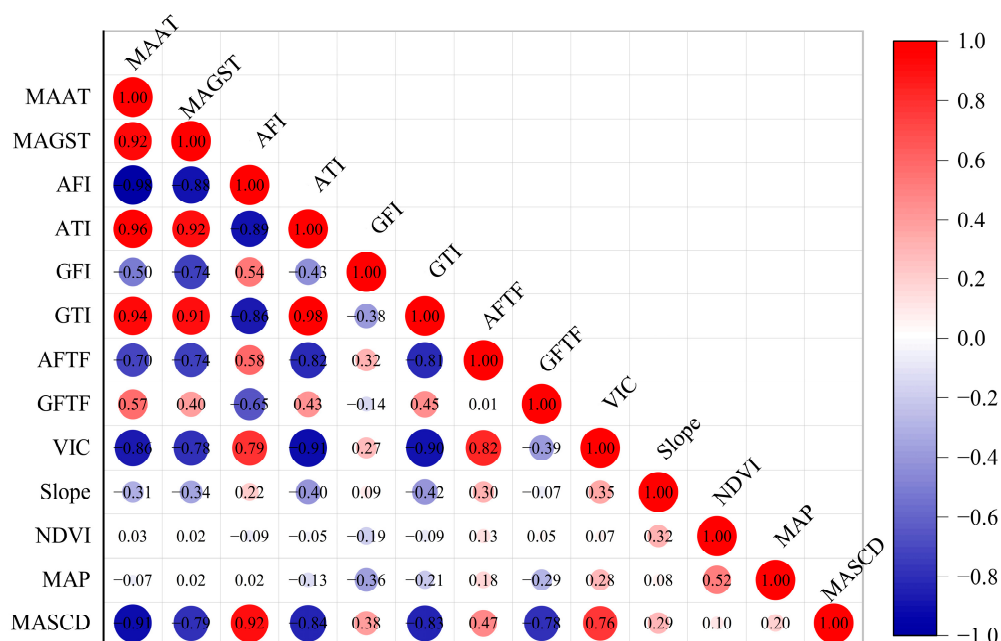


Figure 11. Pearson’s correlation coefficients among the various indices.

Based on Pearson’s correlation coefficient, the evaluation of freezing–thawing hazards in the Daxing’anling forest region and its surrounding 38 meteorological stations was conducted using the eight selected evaluation indices, which were used to create an initial matrix. Table 2 presents the elements of the initial matrix.

**Table 2.** Initial matrix for freezing–thawing hazard assessment in the Daxing’anling forest region.

Meteorological Station	MAGST	GFI	GFTF	VIC	Slope	NDVI	MAP	MASCD
50,136	3.43	1605.26	82.88	25	1.61	0.74	375.61	147.85
50,137	4.20	1458.72	69.44	33	0.25	0.63	375.94	168.95
50,246	3.72	1773.41	89.94	28	2.88	0.60	403.08	140.50
50,247	2.91	1847.53	90.31	39	6.22	0.76	402.71	158.45
50,349	3.09	1770.88	88.88	36	2.11	0.59	423.25	148.90
50,353	3.89	2091.93	81.63	18	0.28	0.65	392.64	140.00
50,425	4.08	2018.53	97.56	22	0.00	0.53	312.52	130.10
50,431	3.49	1590.23	91.38	35	1.02	0.48	387.39	141.05
50,434	2.94	1810.50	97.88	48	0.32	0.59	378.21	145.20
50,442	4.34	1724.55	86.69	18	0.11	0.56	399.78	131.20
50,445	4.29	1624.36	101.69	22	0.28	0.69	400.39	118.15
50,468	6.22	1280.75	81.81	5	1.24	0.77	460.00	130.70
50,514	3.92	2094.52	109.69	8	0.55	0.56	219.06	112.50
50,524	4.54	1977.97	91.81	5	0.05	0.46	255.71	126.40
50,525	4.81	1872.49	86.63	5	0.12	0.46	277.06	131.85
50,526	5.70	1174.96	90.94	14	0.27	0.50	336.95	134.90
50,527	4.71	1797.97	82.13	2	4.10	0.67	261.04	133.00
50,548	5.19	1762.21	94.31	10	0.09	0.65	395.34	111.30
50,557	6.32	1493.43	88.38	6	0.25	0.48	405.38	109.15
50,564	6.86	1102.49	85.19	15	0.00	0.71	448.46	128.45
50,603	5.60	1762.07	108.44	0	0.70	0.34	172.40	100.15
50,618	5.90	1750.66	90.69	6	0.43	0.40	209.98	117.25
50,632	3.96	1660.22	106.75	17	5.91	0.77	377.20	124.85
50,639	6.89	1316.97	116.94	0	0.21	0.38	364.02	57.25
50,645	6.88	1484.71	93.00	0	0.78	0.78	389.71	102.55
50,646	6.86	1526.48	95.38	0	0.19	0.54	394.94	106.95
50,647	7.30	1341.97	112.56	0	0.71	0.81	359.86	86.05
50,655	6.27	1438.43	82.63	8	0.36	0.71	422.38	125.20
50,658	6.91	1392.72	96.88	0	1.25	0.80	413.27	113.85
50,727	5.51	1026.23	90.56	41	3.57	0.65	347.42	149.30
50,739	7.26	1398.04	117.94	0	0.48	0.83	337.83	81.15
50,741	8.38	1184.59	100.94	0	0.21	0.54	354.86	94.80
50,742	8.22	1249.91	95.13	0	0.18	0.67	373.54	93.45
50,745	8.17	1261.14	97.69	0	0.22	0.46	342.45	87.30
50,750	7.69	1132.92	87.44	0	1.03	0.61	393.42	101.00
50,832	7.55	1385.62	138.56	0	0.62	0.73	336.63	66.30
50,833	8.32	1315.75	112.38	0	2.08	0.47	334.62	46.60
50,834	7.07	1378.67	136.31	0	0.34	0.72	327.33	63.70

When evaluating freezing–thawing hazards, we considered that higher values of MAGST, NDVI, and MASCD corresponded to reduced freezing–thawing hazards, so these indicators were positively oriented. In contrast, lower values of GFI, GFTF, VIC, Slope, and MAP indicated reduced freezing–thawing hazards, so these indicators were inversely oriented. Table 3 presents the elements of the standardized decision matrix after applying either positive or inverse orientation.

To determine the weights of each indicator in the evaluation process, we assigned weights to each assessment criterion using the entropy weight method. First, we calculated the entropy value ( $H_{ij}$ ) of each assessment criterion using Equation (6). Then, we calculated the weights ( $w_j$ ) of each criterion using Equation (7). Table 4 presents the entropy values and weights for each assessment criterion.

**Table 3.** Standardized decision matrix for freezing–thawing hazard assessment in the Daxing’anling forest region.

Meteorological Station	MAGST	GFI	GFTF	VIC	Slope	NDVI	MAP	MASCD
50,136	0.0939	0.4580	0.8056	0.4792	0.7405	0.8181	0.2934	0.8275
50,137	0.2359	0.5952	1.0000	0.3125	0.9601	0.5968	0.2923	1.0000
50,246	0.1480	0.3006	0.7034	0.4167	0.5371	0.5219	0.1979	0.7675
50,247	0.0000	0.2312	0.6980	0.1875	0.0000	0.8535	0.1992	0.9142
50,349	0.0317	0.3030	0.7188	0.2500	0.6600	0.5157	0.1278	0.8361
50,353	0.1797	0.0024	0.8237	0.6250	0.9546	0.6238	0.2342	0.7634
50,425	0.2133	0.0711	0.5931	0.5417	1.0000	0.3963	0.5128	0.6825
50,431	0.1063	0.4721	0.6826	0.2708	0.8360	0.2838	0.2525	0.7720
50,434	0.0060	0.2659	0.5886	0.0000	0.9484	0.5183	0.2844	0.8059
50,442	0.2612	0.3463	0.7505	0.6250	0.9818	0.4543	0.2094	0.6915
50,445	0.2520	0.4401	0.5335	0.5417	0.9557	0.7075	0.2073	0.5848
50,468	0.6057	0.7617	0.8210	0.8958	0.8007	0.8769	0.0000	0.6874
50,514	0.1836	0.0000	0.4177	0.8333	0.9119	0.4492	0.8378	0.5386
50,524	0.2977	0.1091	0.6763	0.8958	0.9912	0.2579	0.7103	0.6522
50,525	0.3470	0.2078	0.7514	0.8958	0.9803	0.2458	0.6361	0.6968
50,526	0.5097	0.8608	0.6890	0.7083	0.9566	0.3203	0.4279	0.7217
50,527	0.3292	0.2776	0.8165	0.9583	0.3405	0.6614	0.6918	0.7062
50,548	0.4176	0.3111	0.6401	0.7917	0.9861	0.6213	0.2248	0.5288
50,557	0.6230	0.5627	0.7260	0.8750	0.9594	0.2896	0.1899	0.5112
50,564	0.7217	0.9286	0.7722	0.6875	1.0000	0.7484	0.0401	0.6690
50,603	0.4925	0.3112	0.4358	1.0000	0.8871	0.0000	1.0000	0.4377
50,618	0.5471	0.3219	0.6926	0.8750	0.9310	0.1256	0.8694	0.5774
50,632	0.1912	0.4065	0.4602	0.6458	0.0494	0.8802	0.2879	0.6396
50,639	0.7281	0.7279	0.3128	1.0000	0.9664	0.0972	0.3338	0.0870
50,645	0.7254	0.5708	0.6591	1.0000	0.8738	0.8835	0.2444	0.4573
50,646	0.7231	0.5317	0.6248	1.0000	0.9688	0.4182	0.2262	0.4933
50,647	0.8032	0.7044	0.3761	1.0000	0.8854	0.9423	0.3482	0.3224
50,655	0.6152	0.6142	0.8092	0.8333	0.9425	0.7480	0.1308	0.6424
50,658	0.7310	0.6569	0.6031	1.0000	0.7993	0.9248	0.1625	0.5497
50,727	0.4757	1.0000	0.6944	0.1458	0.4254	0.6260	0.3914	0.8394
50,739	0.7955	0.6520	0.2984	1.0000	0.9229	1.0000	0.4248	0.2824
50,741	1.0000	0.8518	0.5443	1.0000	0.9664	0.4134	0.3656	0.3940
50,742	0.9720	0.7906	0.6284	1.0000	0.9704	0.6655	0.3006	0.3829
50,745	0.9622	0.7801	0.5913	1.0000	0.9645	0.2513	0.4087	0.3327
50,750	0.8746	0.9001	0.7396	1.0000	0.8348	0.5551	0.2315	0.4446
50,832	0.8482	0.6636	0.0000	1.0000	0.9010	0.7867	0.4290	0.1610
50,833	0.9904	0.7290	0.3788	1.0000	0.6651	0.2655	0.4360	0.0000
50,834	0.7602	0.6701	0.0325	1.0000	0.9455	0.7619	0.4613	0.1398

**Table 4.** Entropy values and weights for freezing–thawing hazard assessment in the Daxing’anling forest region.

Index	MAGST	GFI	GFTF	VIC	Slope	NDVI	MAP	MASCD
$H_{ij}$	0.9378	0.9546	0.9779	0.9721	0.9815	0.9647	0.9489	0.9709
$w_j$	0.2132	0.1557	0.0758	0.0959	0.0634	0.1211	0.1751	0.0998

After obtaining the weights for each assessment criterion, we applied Equation (8) to weight the elements in the standard decision matrix, resulting in the weighted standardized matrix. The elements in the weighted standardized matrix are presented in Table 5.



Based on Equations (11) and (12), we calculated the Euclidean distances ( $E_i^+$  and  $E_i^-$ ) for each station and subsequently determined the assessment scores ( $F_i$ ) for each station using Equation (13). To facilitate the classification of freezing–thawing hazards, the assessment scores were normalized. Table 7 provides the Euclidean distances, assessment scores, and normalized assessment scores for each station.

**Table 7.** Euclidean distances, assessment scores, and normalized assessment scores of meteorological stations during freezing–thawing assessment in the Daxing’anling forest region.

Meteorological Station	$E_i^+$	$E_i^-$	$F_i$	Normalized Assessment Scores	Meteorological Station	$E_i^+$	$E_i^-$	$F_i$	Normalized Assessment Scores
50,136	0.0139	0.0100	0.4181	0.2940	50,564	0.0103	0.0145	0.5838	0.7775
50,137	0.0126	0.0109	0.4635	0.4263	50,603	0.0114	0.0134	0.5406	0.6513
50,246	0.0149	0.0078	0.3427	0.0740	50,618	0.0103	0.0131	0.5598	0.7076
50,247	0.0166	0.0086	0.3429	0.0745	50,632	0.0137	0.0093	0.4053	0.2566
50,349	0.0163	0.0076	0.3174	0.0000	50,639	0.0113	0.0128	0.5323	0.6273
50,353	0.0153	0.0089	0.3670	0.1447	50,645	0.0094	0.0137	0.5926	0.8033
50,425	0.0141	0.0089	0.3861	0.2006	50,646	0.0104	0.0126	0.5485	0.6745
50,431	0.0150	0.0080	0.3486	0.0911	50,647	0.0085	0.0148	0.6353	0.9280
50,434	0.0163	0.0078	0.3244	0.0205	50,655	0.0105	0.0127	0.5473	0.6710
50,442	0.0136	0.0089	0.3937	0.2226	50,658	0.0097	0.0140	0.5921	0.8019
50,445	0.0133	0.0092	0.4075	0.2629	50,727	0.0103	0.0130	0.5587	0.7043
50,468	0.0111	0.0136	0.5493	0.6769	50,739	0.0083	0.0149	0.6410	0.9445
50,514	0.0140	0.0110	0.4401	0.3581	50,741	0.0083	0.0161	0.6600	1.0000
50,524	0.0128	0.0109	0.4588	0.4126	50,742	0.0082	0.0160	0.6599	0.9997
50,525	0.0121	0.0109	0.4735	0.4556	50,745	0.0088	0.0155	0.6372	0.9335
50,526	0.0096	0.0127	0.5695	0.7359	50,750	0.0088	0.0154	0.6356	0.9286
50,527	0.0111	0.0118	0.5147	0.5759	50,832	0.0091	0.0147	0.6172	0.8750
50,548	0.0124	0.0099	0.4436	0.3683	50,833	0.0099	0.0152	0.6064	0.8435
50,557	0.0112	0.0116	0.5071	0.5537	50,834	0.0092	0.0141	0.6052	0.8400

After applying the entropy weight–TOPSIS model, we obtained assessment scores for the Daxing’anling forest region and the surrounding meteorological stations. Subsequently, we generated a freezing–thawing evaluation score map (FTE) for the study area using linear interpolation (Figure 12). As shown in Figure 12, FTE gradually decreased from south to north, indicating an increasing severity of freezing–thawing hazards from south to north. However, in Beijicun, the freezing–thawing hazards showed some mitigation. We conducted an analysis of the relationship between FTE and longitude, latitude, and altitude (Equation (23)). The results indicated that FTE was most closely linked to latitude, followed by longitude, with altitude having the lowest effect on FTE.

$$FTE = -0.0200Long - 0.1261Lat - 6.9205 \times 10^4 Alt + 9.5026 (R^2 = 0.77, p < 0.05) \quad (23)$$

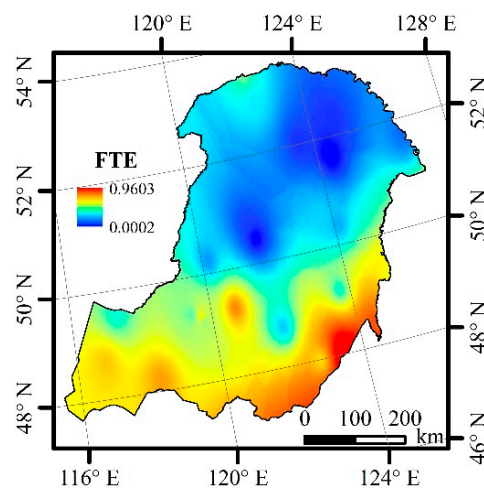


**Figure 12.** Freezing–thawing hazard assessment scores in the Daxing’anling forest region.

## 4. Discussion

### 4.1. Changes in Temperature, Freezing Index, Thawing Index, and Freezing–Thawing Frequency

Between 2005 and 2020, the Daxing'anling forest region experienced a temperature warming rate of  $0.047\text{ }^{\circ}\text{C/a}$ , with the ground temperature rising at a rate of  $0.0695\text{ }^{\circ}\text{C/a}$ . During the same period, the entire northeastern region of China experienced an air temperature increase of  $0.01\text{ }^{\circ}\text{C/a}$ , while the ground surface temperature increased at a rate of  $0.11\text{ }^{\circ}\text{C/a}$  [11]. The thawing of permafrost, which is present in the Daxing'anling forest region, releases significant amounts of greenhouse gases in the context of global climate warming [11,43,44]. This leads to higher greenhouse gas concentrations in the region. Higher gas concentrations are more efficient at absorbing and retaining solar heat, resulting in a higher rate of air temperature increase than in the northeastern region. The Daxing'anling forest region experiences longer snow cover duration, thicker snow, and higher vegetation coverage compared to other parts of northeastern China [45–47]. Snow and vegetation act as insulators, which means that external influences on ground surface temperature in this region are smaller compared to other parts of northeastern China [48,49]. As a result, the rate of ground surface temperature change in this area is lower than that of other northeastern regions. Within the study area, the spatial distribution of MAAT was similar to that of MAGST, and the spatial distribution of the ATCR was similar to that of the GSTCR, although there were numerical differences.

Influenced by air temperature changes, the AFI, ATI, GFI, and GTI in the study area also changed during the study period. The rate of change of the AFI in the Daxing'anling forest region between 2005 and 2020 ( $-12.79\text{ }^{\circ}\text{C}\times\text{d/a}$ ) was insignificantly different from that of northeastern China before 2005 ( $-12.2\text{ }^{\circ}\text{C}\times\text{d/a}$ ). The rate of change of the ATI ( $3.06\text{ }^{\circ}\text{C}\times\text{d/a}$ ) was lower than that of northeastern China before 2005 ( $9.15\text{ }^{\circ}\text{C}\times\text{d/a}$ ). The rate of change of the GFI ( $-22.79\text{ }^{\circ}\text{C}\times\text{d/a}$ ) was lower than that of northeastern China before 2005 ( $-12.3\text{ }^{\circ}\text{C}\times\text{d/a}$ ). The rate of change of the GTI ( $0.99\text{ }^{\circ}\text{C}\times\text{d/a}$ ) was lower than that of northeastern China before 2005 ( $11.3\text{ }^{\circ}\text{C}\times\text{d/a}$ ) [33]. Since the freezing–thawing index is an indicator of permafrost change, this means that permafrost in the Daxing'anling forest region may have degraded at an alarming rate between 2005 and 2020, and this degradation rate is increasing.

In the context of ongoing global warming, the AFTF in the Daxing'anling forest region was increasing at a rate of  $0.48\text{ th/a}$ . This implies that buildings exposed to the air in this region are experiencing an increasing number of freezing–thawing cycles each year. In contrast, the GFTF was decreasing at a rate of  $0.75\text{ th/a}$ , which is lower than the overall Daxing'anling's GFTF decline rate of  $2.0\text{ th/a}$  [35]. This difference is due to changes in data collection methods. Prior to 2005, ground surface temperature measurements were obtained manually, whereas after 2005, automatic measurements were employed. Manual measurements collected temperature data from the surface of the snow, while automatic measurements obtained data from beneath the snow [50]. Consequently, the data obtained for GFTF change rates are lower with the latter method.

In multiple linear regressions using longitude, latitude, and elevation as independent variables and the MAAT, MAGST, AFI, ATI, GFI, GTI, AFTE, and GFTF as dependent variables, we found that latitude played a dominant role in influencing these factors, with longitude having an intermediate influence and elevation contributing the least.

### 4.2. Freezing–Thawing Hazard Assessment

Based on the freezing–thawing assessment scores, the freezing–thawing hazards in the study area were categorized into five levels: very dangerous, dangerous, moderately dangerous, safe, and very safe, corresponding to levels I to V. Table 8 shows the classifications and ratios of freezing–thawing hazards in the Daxing'anling forest region. The freezing–thawing hazard classification levels of different regions are depicted in Figure 13. With the exception of the areas near  $48^{\circ}\text{ N}$  latitude, most regions are situated within a relatively dangerous freezing–thawing hazard environment. Specifically, a significant portion of the areas north of  $50^{\circ}\text{ N}$  latitude, covering 55.66% of the entire study area,

falls into the dangerous and very dangerous categories. Consequently, it is imperative to consider the assessment of freezing–thawing hazards in the region north of 50° N latitude during engineering activities. In regions with higher freezing–thawing hazard levels, road surface damage due to freezing and thawing is notably more pronounced than in other areas. Figure 13 displays instances of freezing–thawing hazards in Mo’he (a) and Tulihe (b). According to this study, Mo’he is classified as level II (dangerous) in terms of freezing–thawing hazards, while Tulihe is classified as level I (very dangerous). Moreover, in regions with severe freezing–thawing hazards, the exteriors of buildings are more susceptible to cracking and spalling.

**Table 8.** Classifications and ratios of freezing–thawing hazards in the Daxing’anling forest region.

Disaster State	Scoring Set	Level	Ratio
Very dangerous	0~0.2	I	23.68%
Dangerous	0.2~0.4	II	31.98%
Moderately dangerous	0.4~0.6	III	26.17%
Safe	0.6~0.8	IV	16.92%
Very safe	0.8~1.0	V	1.25%

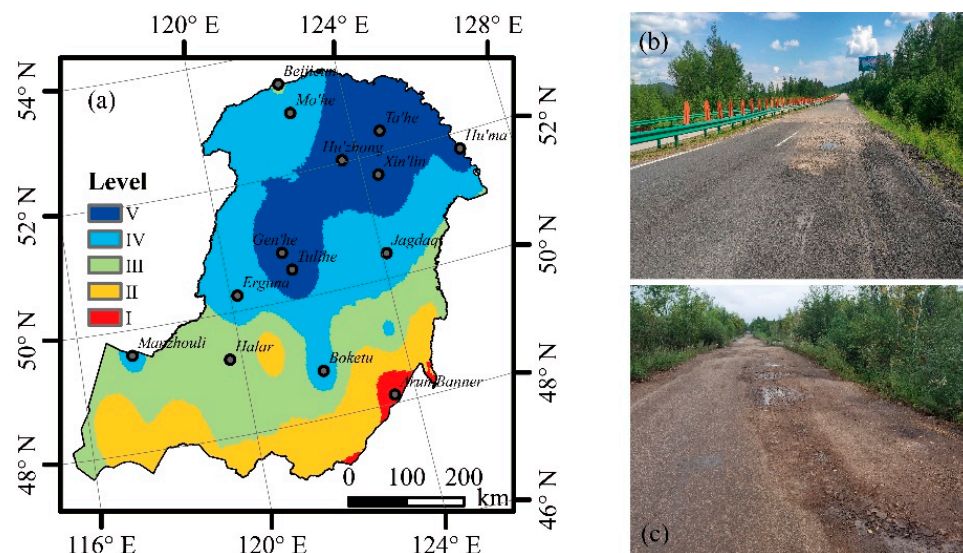


**Figure 13.** Freezing–thawing hazard classification in the Daxing’anling forest region. (a) Map of freezing–thawing hazard classification; (b) freezing–thawing hazard on a road in Mo’he; (c) freezing–thawing hazard on a road in Tulihe.

### 5. Conclusions

From 2005 to 2020, the air temperature in the Daxing’anling forest region increased at a rate of 0.047 °C/a, which is higher than in the entire northeastern region. Due to the influence of snow cover and vegetation, ground surface temperature increased at a rate of 0.0695 °C/a, which is lower than in the entire northeastern region. Within the study area, the spatial distributions of MAAT and MAGST were similar, with both decreasing from south to north.

We calculated the rates of change for the AFI, ATI, GFI, and GTI and their spatial distributions. Considering their overall trends, we conclude that permafrost in the Daxing’anling forest region is degrading at an unprecedented rate. Additionally, we collected data on the AFTF and GFTF and their rates of change, which indicated an increasing number of freezing–thawing cycles for structures exposed to the air. Latitude had the strongest effect on the MAAT, MAGST, AFI, ATI, GFI, GTI, AFTF, and GFTF, followed by longitude and elevation.

The assessment results indicated that most areas north of 50° N latitude are experiencing dangerous or extremely dangerous freezing–thawing hazards.

**Author Contributions:** Conceptualization, K.C. and S.H.; data curation, K.C.; formal analysis, K.C.; funding acquisition, K.C.; investigation, K.C.; methodology, K.C. and S.H.; project administration, K.C.; resources, K.C.; software, K.C.; supervision, S.H.; validation, K.C. and S.H.; visualization, K.C.; writing—original draft, K.C.; writing—review and editing, K.C. All authors have read and agreed to the published version of the manuscript.

**Funding:** This research was funded by the Innovation Foundation for Doctoral Program of Forestry Engineering of Northeast Forestry University (LYGC202207).

**Institutional Review Board Statement:** Not applicable.

**Informed Consent Statement:** Not applicable.

**Data Availability Statement:** No new data were created or analyzed in this study. Data sharing is not applicable to this article.

**Conflicts of Interest:** The authors declare no conflict of interest.

## References

- Zhong, X. Study of Protection and Construction of Mountain Ecological Security Barrier in China. *J. Mt. Sci.* **2008**, *26*, 2–11.
- Jin, H.; Hao, J.; Chang, X.; Zhang, J.; Yu, Q.; Qi, J.; Lü, L.; Wang, S. Zonation and Assessment of Frozen-Ground Conditions for Engineering Geology along the China–Russia Crude Oil Pipeline Route from Mo’he to Daqing, Northeastern China. *Cold Reg. Sci. Technol.* **2010**, *64*, 213–225. [[CrossRef](#)]
- Lu, Y.; Yu, W.; Guo, M.; Liu, W. Spatiotemporal Variation Characteristics of Land Cover and Land Surface Temperature in Mohe County, Heilongjiang Province. *J. Glaciol. Geocryol.* **2017**, *39*, 1137–1149.
- Wang, F.; Li, G.; Ma, W.; Mu, Y.; Zhou, Z.; Mao, Y. Permafrost Thawing along the China-Russia Crude Oil Pipeline and Countermeasures: A Case Study in Jiagedaqi, Northeast China. *Cold Reg. Sci. Technol.* **2018**, *155*, 308–313. [[CrossRef](#)]
- Li, P.; Qian, H.; Howard, K.W.F.; Wu, J. Building a New and Sustainable “Silk Road Economic Belt”. *Environ. Earth Sci.* **2015**, *74*, 7267–7270. [[CrossRef](#)]
- Ren, W.; Xue, B.; Yang, J.; Lu, C. Effects of the Northeast China Revitalization Strategy on Regional Economic Growth and Social Development. *Chin. Geogr. Sci.* **2020**, *30*, 791–809. [[CrossRef](#)]
- Jin, H.; Yu, Q.; Lü, L.; Guo, D.; He, R.; Yu, S.; Sun, G.; Li, Y. Degradation of Permafrost in the Xing’anling Mountains, Northeastern China. *Permafrost Periglac. Process.* **2007**, *18*, 245–258. [[CrossRef](#)]
- Wei, Z.; Jin, H.; Zhang, J.; Yu, S.; Han, X.; Ji, Y.; He, R.; Chang, X. Prediction of Permafrost Changes in Northeastern China under a Changing Climate. *Sci. China Earth Sci.* **2011**, *54*, 924–935. [[CrossRef](#)]
- Guo, D.; Li, D.; Hua, W. Quantifying Air Temperature Evolution in the Permafrost Region from 1901 to 2014. *Int. J. Climatol.* **2018**, *38*, 66–76. [[CrossRef](#)]
- Li, X.; Jin, H.; Wang, H.; Wu, X.; Huang, Y.; He, R.; Luo, D.; Jin, X. Distributive Features of Soil Carbon and Nutrients in Permafrost Regions Affected by Forest Fires in Northern Da Xing’anling (Hinggan) Mountains, NE China. *Catena* **2020**, *185*, 104304. [[CrossRef](#)]
- Li, X.; Jin, H.; Sun, L.; Wang, H.; He, R.; Huang, Y.; Chang, X. Climate Warming over 1961–2019 and Impacts on Permafrost Zonation in Northeast China. *J. For. Res.* **2022**, *33*, 767–788. [[CrossRef](#)]
- Wang, W.; Jin, X.; Jin, H.; Li, X.; Wang, X.; He, R.; Li, Y.; Li, X.; Wang, L.; Wang, W.; et al. Evaluation of Ground Surface Deformation in Discontinuous Permafrost Regions along the China-Russia Crude Oil Pipelines in Northeast China Using InSAR and Ground Surveys. *Eng. Geol.* **2023**, *323*, 107227. [[CrossRef](#)]
- Han, L.; Tsunekawa, A.; Tsubo, M. Monitoring Near-Surface Soil Freeze-Thaw Cycles in Northern China and Mongolia from 1998 to 2007. *Int. J. Appl. Earth Obs. Geoinf.* **2010**, *12*, 375–384. [[CrossRef](#)]
- Zhao, Y.; Wang, E.; Cruse, R.M.; Chen, X. Characterization of Seasonal Freeze-Thaw and Potential Impacts on Soil Erosion in Northeast China. *Can. J. Soil Sci.* **2012**, *92*, 567–571. [[CrossRef](#)]
- Zhang, S.; Zhao, B. Research on the Performance of Concrete Materials under the Condition of Freeze-Thaw Cycles. *Eur. J. Environ. Civ. Eng.* **2013**, *17*, 860–871. [[CrossRef](#)]
- Lin, H.; Han, Y.; Liang, S.; Gong, F.; Han, S.; Shi, C.; Feng, P. Effects of Low Temperatures and Cryogenic Freeze-Thaw Cycles on Concrete Mechanical Properties: A Literature Review. *Constr. Build. Mater.* **2022**, *345*, 128287. [[CrossRef](#)]
- Hwang, C.-L.; Yoon, K. *Multiple Attribute Decision Making: Methods and Applications*; Lecture Notes in Economics and Mathematical Systems; Springer: Berlin/Heidelberg, Germany, 1981; Volume 186, ISBN 978-3-540-10558-9.
- Saaty, R.W. The Analytic Hierarchy Process—What It Is and How It Is Used. *Math. Model.* **1987**, *9*, 161–176. [[CrossRef](#)]
- Ho, W.; Ma, X. The State-of-the-Art Integrations and Applications of the Analytic Hierarchy Process. *Eur. J. Oper. Res.* **2018**, *267*, 399–414. [[CrossRef](#)]

20. Kabir, S.; Papadopoulos, Y. A Review of Applications of Fuzzy Sets to Safety and Reliability Engineering. *Int. J. Approx. Reason.* **2018**, *100*, 29–55. [[CrossRef](#)]
21. Kumar, R.; Singh, S.; Bilga, P.S.; Jatin; Singh, J.; Singh, S.; Scutaru, M.-L.; Pruncu, C.I. Revealing the Benefits of Entropy Weights Method for Multi-Objective Optimization in Machining Operations: A Critical Review. *J. Mater. Res. Technol.* **2021**, *10*, 1471–1492. [[CrossRef](#)]
22. Liu, X.; Yang, W.; Zhang, X. Rockburst Prediction of Multi-Dimensional Cloud Model Based on Improved Hierarchical Analytic Method and Critic Method. *J. Hunan Univ. (Nat. Sci.)* **2021**, *48*, 118–124. [[CrossRef](#)]
23. Jalilibal, Z.; Amiri, A.; Castagliola, P.; Khoo, M.B.C. Monitoring the Coefficient of Variation: A Literature Review. *Comput. Ind. Eng.* **2021**, *161*, 107600. [[CrossRef](#)]
24. Ren, Z. Evaluation Method of Port Enterprise Product Quality Based on Entropy Weight TOPSIS. *J. Coast. Res.* **2020**, *103*, 766–769. [[CrossRef](#)]
25. Li, X. TOPSIS Model with Entropy Weight for Eco Geological Environmental Carrying Capacity Assessment. *Microprocess. Microsyst.* **2021**, *82*, 103805. [[CrossRef](#)]
26. Yuan, S. Determinants of Nutrients and Stoichiometric Characteristics of Soil in Daxing'an Forest. Ph.D. Thesis, Northeast Forestry University, Harbin, China, 2019.
27. Li, X.; Jin, H.; Wang, H.; Jin, X.; Bense, V.F.; Marchenko, S.S.; He, R.; Huang, Y.; Luo, D. Effects of Fire History on Thermal Regimes of Permafrost in the Northern Da Xing'anling Mountains, NE China. *Geoderma* **2022**, *410*, 115670. [[CrossRef](#)]
28. Li, W.; Jiang, Y.; Dong, M.; Du, E.; Wu, F.; Zhao, S.; Xu, H. Species-Specific Growth-Climate Responses of Dahurian Larch (*Larix gmelinii*) and Mongolian Pine (*Pinus sylvestris* Var. *Mongolica*) in the Greater Khingan Range, Northeast China. *Dendrochronologia* **2021**, *65*, 125803. [[CrossRef](#)]
29. Liu, Y.; Trancoso, R.; Ma, Q.; Ciais, P.; Gouvêa, L.P.; Yue, C.; Assis, J.; Blanco, J.A. Carbon Density in Boreal Forests Responds Non-Linearly to Temperature: An Example from the Greater Khingan Mountains, Northeast China. *Agric. For. Meteorol.* **2023**, *338*, 109519. [[CrossRef](#)]
30. Huang, S.; Ding, Q.; Chen, K.; Hu, Z.; Liu, Y.; Zhang, X.; Gao, K.; Qiu, K.; Yang, Y.; Ding, L. Changes in Near-Surface Permafrost Temperature and Active Layer Thickness in Northeast China in 1961–2020 Based on GIPL Model. *Cold Reg. Sci. Technol.* **2023**, *206*, 103709. [[CrossRef](#)]
31. Zhang, Z.; Li, M.; Wang, J.; Yin, Z.; Yang, Y.; Xun, X.; Wu, Q. A Calculation Model for the Spatial Distribution and Reserves of Ground Ice—A Case Study of the Northeast China Permafrost Area. *Eng. Geol.* **2023**, *315*, 107022. [[CrossRef](#)]
32. Frauenfeld, O.W.; Zhang, T.; McCreight, J.L. Northern Hemisphere Freezing/Thawing Index Variations over the Twentieth Century. *Int. J. Climatol.* **2007**, *27*, 47–63. [[CrossRef](#)]
33. Luo, D.; Jin, H.; Jin, R.; Yang, X.; Lü, L. Spatiotemporal Variations of Climate Warming in Northern Northeast China as Indicated by Freezing and Thawing Indices. *Quat. Int.* **2014**, *349*, 187–195. [[CrossRef](#)]
34. Ma, S.; Zhao, J.; Chen, J.; Zhang, S.; Dong, T.; Mei, Q.; Hou, X.; Liu, G. Ground Surface Freezing and Thawing Index Distribution in the Qinghai-Tibet Engineering Corridor and Factors Analysis Based on GeoDetector Technique. *Remote Sens.* **2023**, *15*, 208. [[CrossRef](#)]
35. Wei, H.; Zhang, Z.; Melnikov, A.; Jin, D.; Gao, S.; Feng, W. Distribution law of annual freeze-thaw frequency in Xing'anling region of Northeast China. *J. Glaciol. Geocryol.* **2022**, *44*, 415–426. [[CrossRef](#)]
36. Zyoud, S.H.; Fuchs-Hanusch, D. A Bibliometric-Based Survey on AHP and TOPSIS Techniques. *Expert Syst. Appl.* **2017**, *78*, 158–181. [[CrossRef](#)]
37. Salih, M.M.; Zaidan, B.B.; Zaidan, A.A.; Ahmed, M.A. Survey on Fuzzy TOPSIS State-of-the-Art between 2007 and 2017. *Comput. Oper. Res.* **2019**, *104*, 207–227. [[CrossRef](#)]
38. Shannon, C.E. A Mathematical Theory of Communication. *Bell Syst. Tech. J.* **1948**, *27*, 379–423. [[CrossRef](#)]
39. Oluah, C.; Akinlabi, E.T.; Njoku, H.O. Selection of Phase Change Material for Improved Performance of Trombe Wall Systems Using the Entropy Weight and TOPSIS Methodology. *Energy Build.* **2020**, *217*, 109967. [[CrossRef](#)]
40. Topcu, E. Drought Analysis Using the Entropy Weight-Based TOPSIS Method: A Case Study of Kars, Turkey. *Russ. Meteorol. Hydrol.* **2022**, *47*, 224–231. [[CrossRef](#)]
41. Le Roux, D.; Olivès, R.; Neveu, P. Combining Entropy Weight and TOPSIS Method for Selection of Tank Geometry and Filler Material of a Packed-Bed Thermal Energy Storage System. *J. Clean. Prod.* **2023**, *414*, 137588. [[CrossRef](#)]
42. Afyouni, S.; Smith, S.M.; Nichols, T.E. Effective Degrees of Freedom of the Pearson's Correlation Coefficient under Autocorrelation. *NeuroImage* **2019**, *199*, 609–625. [[CrossRef](#)]
43. Ran, Y.; Li, X.; Cheng, G.; Zhang, T.; Wu, Q.; Jin, H.; Jin, R. Distribution of Permafrost in China: An Overview of Existing Permafrost Maps. *Permafrost Periglacial Process.* **2012**, *23*, 322–333. [[CrossRef](#)]
44. Chen, S.; Zang, S.; Sun, L. Characteristics of permafrost degradation in Northeast China and its ecological effects: A review. *Sci. Cold Arid. Reg.* **2020**, *12*, 1–11.
45. Mao, D.; Wang, Z.; Luo, L.; Ren, C. Integrating AVHRR and MODIS Data to Monitor NDVI Changes and Their Relationships with Climatic Parameters in Northeast China. *Int. J. Appl. Earth Obs. Geoinf.* **2012**, *18*, 528–536. [[CrossRef](#)]
46. Chen, S.; Yang, Q.; Xie, H.; Zhang, H.; Lu, P.; Zhou, C. Spatiotemporal Variations of Snow Cover in Northeast China Based on Flexible Multiday Combinations of Moderate Resolution Imaging Spectroradiometer Snow Cover Products. *J. Appl. Remote Sens.* **2014**, *8*, 084685. [[CrossRef](#)]

47. Li, H.; Zhong, X.; Zheng, L.; Hao, X.; Wang, J.; Zhang, J. Classification of Snow Cover Persistence across China. *Water* **2022**, *14*, 933. [[CrossRef](#)]
48. Zhao, J.; Chen, J.; Wu, Q.; Hou, X. Snow Cover Influences the Thermal Regime of Active Layer in Urumqi River Source, Tianshan Mountains, China. *J. Mt. Sci.* **2018**, *15*, 2622–2636. [[CrossRef](#)]
49. Way, R.G.; Lapalme, C.M. Does Tall Vegetation Warm or Cool the Ground Surface? Constraining the Ground Thermal Impacts of Upright Vegetation in Northern Environments. *Environ. Res. Lett.* **2021**, *16*, 054077. [[CrossRef](#)]
50. Li, X.; Jin, H.; Sun, L.; Wang, H.; Huang, Y.; He, R.; Chang, X.; Yu, S.; Zang, S. TTOP-Model-Based Maps of Permafrost Distribution in Northeast China for 1961–2020. *Permafr. Periglac. Process.* **2022**, *33*, 425–435. [[CrossRef](#)]

**Disclaimer/Publisher’s Note:** The statements, opinions and data contained in all publications are solely those of the individual author(s) and contributor(s) and not of MDPI and/or the editor(s). MDPI and/or the editor(s) disclaim responsibility for any injury to people or property resulting from any ideas, methods, instructions or products referred to in the content.